Bulk (100) scandium nitride crystal growth by sublimation on tungsten single crystal seeds

Hayder A. Al-Atabi, Neelam Khan, Edil Nour, Joseph Mondoux, Yi Zhang, and J. H. Edgar

Citation: Appl. Phys. Lett. **113**, 122106 (2018); doi: 10.1063/1.5051457
View online: https://doi.org/10.1063/1.5051457
View Table of Contents: http://aip.scitation.org/toc/apl/113/12
Published by the American Institute of Physics

Bulk (100) scandium nitride crystal growth by sublimation on tungsten single crystal seeds

Hayder A. Al-Atabi,[1,2] Neelam Khan,[3] Edil Nour,[3] Joseph Mondoux,[3] Yi Zhang,[4] and J. H. Edgar[1,a)]
[1]Department of Chemical Engineering, Kansas State University, Manhattan, Kansas 66506, USA
[2]Chemical Engineering Department, The University of Technology, Baghdad, Iraq
[3]School of Science and Technology, Georgia Gwinnett College, Lawrenceville, Georgia 30043, USA
[4]Nitride Solutions Inc., 3333 West Pawnee Street, Wichita, Kansas 67213, USA

(Received 8 August 2018; accepted 6 September 2018; published online 20 September 2018)

Scandium nitride single crystals (14–90 μm thick) were grown on a tungsten (100) single crystal substrate by physical vapor transport in the temperature range of 1850 °C–2000 °C and pressure of 15–35 Torr. Epitaxial growth was confirmed using in-plane ϕ scan and out-of-plane x-ray diffraction techniques which revealed that ScN exhibits cube-on-cube growth with a plane relationship ScN (001) || W (001) and normal direction ScN [100] || W [110]. Atomic force microscopy revealed that the surface roughness decreased from 83 nm to 18 nm as the growth temperature was increased. The x-ray diffraction rocking curve (XRC) widths decreased with temperature, indicating that the crystal quality improved as the growth temperature increased. The lowest XRC FWHM was 821 arcsec which is so far the lowest value reported for ScN. Scanning electron microscopy exhibited the formation of macrosteps and cracks on the crystal surface with the latter due to the mismatch of ScN and tungsten coefficients of thermal expansion. *Published by AIP Publishing.* https://doi.org/10.1063/1.5051457

Recently, there has been a remarkable interest in the properties and applications of transition metal nitrides.[1] In particular, the crystal growth and characterization of the group IIIB transition metal nitride scandium nitride (ScN), a semiconductor, is of interest for both fundamental science and potential electronic device applications. It possesses excellent physical properties such as high hardness, mechanical strength, and outstanding electronic transport properties. The heat, free energy, and entropy of formation of ScN suggest its high thermal stability. Its melting point is $\geq$2600 °C.[2] It has the rock salt crystal structure with a lattice constant of 4.503 ± 0.002 Å.[2–7] It has a direct bandgap of 2.0 eV and an indirect band gap of 0.9 eV[8] and typically has a high electron carrier concentration ($>10^{20}$ cm^{-3}).[4,9] One of the most exciting aspects of ScN is that it can have either *n*-type or *p*-type conductivity (with magnesium doping).[10] The electrical properties of ScN are sensitive to impurities.[10] The electrical resistivity of unintentionally doped ScN varies dramatically with reported values of 25, 130, 308, and 461 $\mu\Omega$ cm by Samsonov *et al.*,[11] Sclar,[12] Gschneidner,[13] and Dismukes *et al.*,[3,4] respectively.

Scandium nitride has several potential device applications. Moram *et al.*[14] and Lupina *et al.*[15] used ScN as a buffer layer on Si substrate to support the subsequent growth of GaN. Free-standing ScN crystals could serve as lattice-matched, electrically conductive substrates for other semiconductors such as zinc blende GaN (a = 4.52 Å)[16] and boron phosphide (a = 4.55 Å).[17] ScN could also be utilized for high temperature ohmic contacts to IIIA nitrides.[18] Large piezoelectric coefficients can be achieved by alloying scandium nitride with aluminum nitride.[19,20] For all of these applications, control over the material's structure and crystal quality is essential.

It has proven to be difficult to produce high quality ScN layers and bulk crystals for several reasons. First, the maximum temperature employed in epitaxial growth studies has been relatively low, 1100 °C for hydride vapor phase epitaxy (HVPE),[21] 1050 °C for molecular beam epitaxy,[22] and 950 °C for reactive magnetron sputtering. Such low temperatures result in thin films (<1 μm) with small grain sizes, i.e., high densities of grain boundaries. Second, defects and cracking are often caused by the mismatch of substrate and ScN layer properties (crystal structure, lattice constants, and coefficients of thermal expansion).

ScN has been deposited on many different substrates. Gall *et al.*[23] produced ScN(001) single crystals on MgO(001) and TiN(001) buffer layers on MgO(001) by ultrahigh vacuum reactive magnetron sputter deposition. Ohgaki *et al.*[24] also synthesized ScN films on MgO(110) and α-$Al_2O_3(10\bar{1}0)$ substrates by (MBE), and x-ray diffraction (XRD) revealed ScN(220) for both substrates. Edgar *et al.*[21] used (HVPE) to deposit ScN on 6H-SiC(0001) and reported that ScN exhibited (111) orientation and a mixture of (100) and (111) orientations at substrate temperatures of 800–900 °C and 1000–1100 °C, respectively. Moram *et al.*[25] grew epitaxial 100-oriented ScN films on 100-oriented Si and mixed orientation of ScN(111) and (100) on Si(111) via the (MBE) growth method. Inevitably, this heteroepitaxy results in high dislocation densities and cracking of the films.

Here, we demonstrate two advances: the use of physical vapor transport (PVT) for preparing epitaxial ScN layers and a single crystal tungsten (100) substrate. The PVT technique is widely employed for the bulk crystal growth of silicon carbide[26] and aluminum nitride.[27]

a)Author to whom correspondence should be addressed: edgarjh@ksu.edu

The present study builds on our previous work,[2] in which polycrystalline ScN was grown on polycrystalline tungsten foil, by employing (100) tungsten single crystal seeds to produce the ScN single crystal. The lattice constant mismatch was minimized by this orientation preference between the ScN crystal and the tungsten seed. The lattice constant of tungsten is 3.165 Å and about ~4.49–4.51 Å for ScN. The directed cube-on-cube lattice mismatch is very large, 42.18% (based on tungsten). However, rotating the unit cell by 45° and considering the square that is formed by the nearest 4 tungsten atoms (Fig. 1) produce a new square. The diagonal of this new square is about 4.48 Å, thus reducing the mismatch dramatically to 0.3% (based on tungsten). Therefore, the ScN crystal orients on tungsten to minimize the lattice mismatch. A 45° angle exists between the ScN and tungsten unit cells and results in a plane relationship ScN (001) || W (001) with normal direction ScN [100] || W [110]. This orientational relationship also occurs with titanium nitride on tungsten.[28]

The sublimation growth was conducted in a tungsten heating element furnace with a maximum temperature of 2400 °C. Tungsten previously proved to be a good unreactive metal for the sublimation growth of TiN[28] and ErN,[29] so it was used as a substrate for the deposited ScN crystals and to manufacture crucibles used in the experiments.

Ultra-high-purity gases, nitrogen (99.999% N_2) and forming gas (95% Ar and 5% H_2), were used in the experiments. The nitrogen and forming gases were further purified with inline moisture and oxygen purifiers to reduce the impurity concentrations from the ppm level to the ppb level. Baking in forming gas helped to reduce and to remove oxygen present as native oxides on the surface of the ScN source, the crucible, and the substrate (the tungsten seed). During the baking stage, the furnace was held at 1000 °C for 2 h. The ScN source was synthesized by heating small chunks of pure Sc metal (99.9% purity) in ultra-high-purity nitrogen at 1100 °C and 500 Torr for 10 h.

The ScN crystal was grown on a single crystal tungsten seed with a (100) orientation. The tungsten seed was mechanically polished to achieve an optical surface. Cleaning with distilled water, acetone, methanol, and isopropanol sequentially in an ultrasonic cleaner followed the polishing process.

The sublimation was carried out in the temperature range of 1850 °C–2000 °C and pressure range of 15–35 Torr in the ultra-high-purity nitrogen gas. The growth time varied from 100 h to 360 h. The grown ScN crystals were carefully detached from the tungsten seed with a razor blade.

A Rigaku MiniFlex II diffractometer was employed to determine the orientation and lattice constants of the ScN layer by θ-2θ x-ray diffraction. To confirm the epitaxial growth, XRD ϕ scans were taken using a Rigaku Smartlab diffractometer. To establish epitaxy, the dome reflections of film and substrate peaks were needed to ensure that they are oriented as expected from their crystal symmetry. To do so, the x-ray detector was fixed at $2\theta = 39.9°$, the location of the ScN (200) peak. The post-growth seed (ScN crystal upon W seed) was rotated 360°. Then, the x-ray detector was fixed at $2\theta = 40.2°$ which represents the diffraction of the W (110) plane, and at 360°, the post-growth seed was rotated again. The 45° angle rotation relationship between the ScN film and W seed was confirmed with a Bruker D8 Discover diffractometer. In this measurement, the ScN crystal upon the W seed was rotated to $2\theta = 40.2°$ which represents W (220) orientation. Then, it was rotated to $2\theta = 57.7°$ which represents ScN (220) orientation.

To determine the structural quality ScN, the rocking curve scan was performed to calculate the Full Width at Half Maximum (FWHM) of the ScN (200) peak.

High magnification images of the ScN layer were taken with a scanning electron microscope (SEM) to determine the crystal surface morphology and defects such as steps and cracks.

The surface topography and roughness of the ScN crystal were investigated by atomic force microscopy (AFM).

For a ScN crystal removed from the tungsten substrate, only two peaks were evident, the (200) and (400) reflections, at 39.9° and 86.2°, respectively, in the XRD θ-2θ pattern (Fig. 2). This suggests that only ScN single crystal of the (100) family was produced.

The FWHMs of θ-2θ scans decrease as the growth temperature increases, showing that the crystallinity of ScN films improved at higher growth temperature (the insets in Fig. 2). This was due to greater atom mobility at higher temperatures and the tendency of threading dislocation to recombine with the increasing layer thickness.

In the XRD ϕ scans (not shown) at 39.9° ($ScN_{(200)}$) and 40.2° ($W_{(110)}$) detector positions, peaks appeared at ϕ values

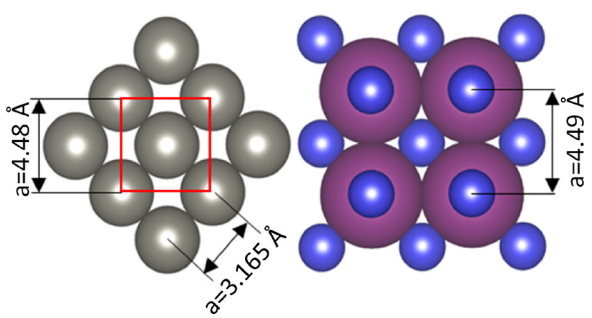

FIG. 1. A schematic representation of ScN (200) crystals grown on (200) tungsten. Dark gray spheres are tungsten, and large purple spheres and small blue spheres are Sc and N, respectively.

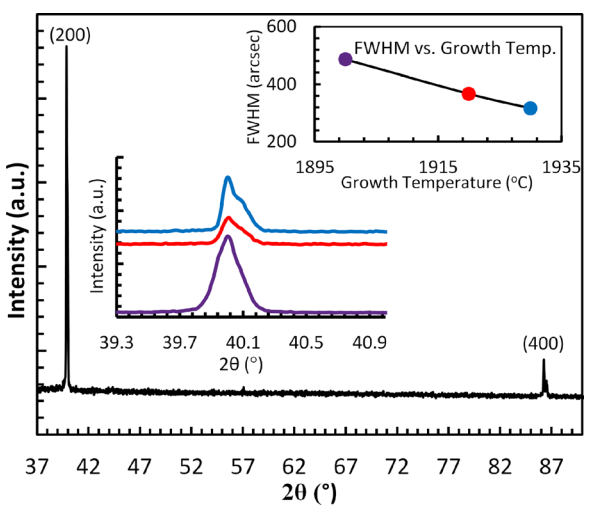

FIG. 2. θ-2θ XRD pattern for the ScN crystal grown at 1930 °C and 15 Torr. The insets are the FWHMs of ScN (200) at different temperatures.

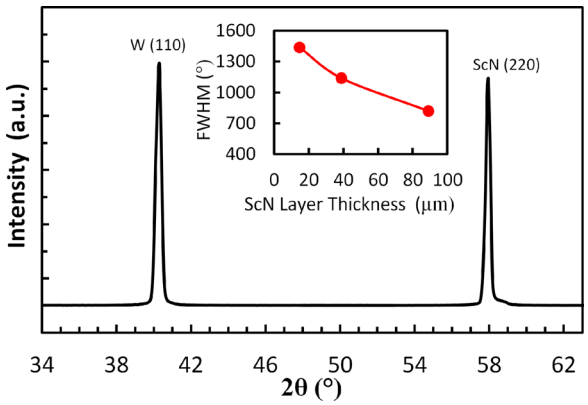

FIG. 3. XRD pattern for 45° (200) plane rotation. The inset is the effect of the ScN layer thickness on the FWHM of the x-ray rocking curve.

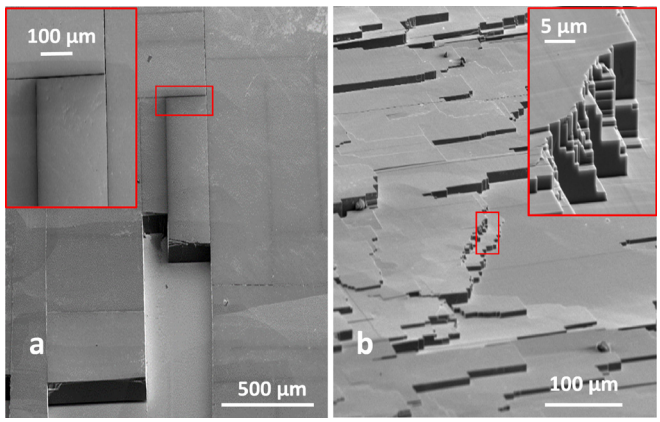

FIG. 4. The SEM images of ScN. (a) shows the cracking of the ScN crystal grown at 1950 °C and 35 Torr due to the difference in the thermal expansion coefficient. (b) Is ScN grown at 1900 °C and 15 Torr showing that the steps formed on the crystal surface.

of 17°, 107°, 197°, and 287°. For $ScN_{(200)}$, the peaks had different intensities, and this is related to the steps presenting on the crystal surface, which will be explained later. For $W_{(110)}$, the peaks were not intense because the ScN layer had steps and was so thick and blocked the x-rays from reaching the tungsten substrate.

XRD analysis of the ScN layer and the tungsten single crystal revealed an orientational relationship of ScN (001) || W (001) with normal direction ScN [100] || W [110], a 45° rotation between the ScN and W lattices, as defined by their primary unit cell directions [100]. The ScN (200) planes are parallel to the substrate surface when the tungsten seed (100) is parallel to the growth surface. However, the tungsten substrate surface was unintentionally slightly tilted away from the (100) plane during cutting and machining the seed. This resulted in ScN surfaces with steps, but the ScN planes were still parallel with the tungsten (100) plane, and with the in-plane directions ScN [100] || W [110]. To confirm this, the in-plane XRD pattern of ScN (220) and W (110) was performed as shown in Fig. 3. When the post-growth ScN(100) on the W(100) composite was tilted 45°, only two x-ray diffraction peaks were evident: one at $2\theta = 57.7°$ from the ScN(220) plane (ScN (100) plane with 45° tilt) and the other at $2\theta = 40.2°$ which is for W(110) plane (underlying W(100) plane with 45° tilt). This confirms that the planes (100) of the ScN and W were parallel, with a 45° angle between the perpendicular ScN [200] and W [110] directions.

The crystal quality greatly improved with the ScN layer thickness, as evidenced by the decreasing FWHM of x-ray rocking curves (the inset in Fig. 3). With the ScN layer thickness ranging from 14 to 90 μm, the FWHM decreased from 1438 to 821 arcsec. This improving crystal quality is attributable to a reduction in the dislocation density. The dislocations with opposite Burger's vectors are attracted toward each other as the ScN layer becomes thicker and ultimately combine and are annihilated. Although the XRD ω-2θ pattern revealed a relatively wide FWHM compared to the conventional high quality semiconductors, the ScN grown in this work has the lowest value reported up to date. The XRD ω-2θ pattern revealed a relatively wide FWHM for the tungsten seed, which consequently affected the quality of the ScN crystal. Table I lists the previously reported FWHMs for XRC peaks taken from ScN films.

The mismatch in the thermal expansions between the ScN layer and the tungsten seed generated stresses, resulting in cracks on the ScN crystal. Figure 4(a) shows how the cracks were oriented regularly generating square and rectangular shapes of the ScN crystal.

No individual grain boundaries are apparent in the SEM image, but large macrosteps, several microns high, can be seen on the ScN surfaces, as a result of step bunching [Fig. 4(b)]. In general, step bunching can be caused by the misorientation of the substrate surface from the (100) plane, substrate polishing damage, and extended defects running through the ScN layer. Step bunching is caused by a difference between the distance of neighboring kinks and the

TABLE I. FWHM of the rocking curve for the ScN single crystal.

Growth method	Growth Temp. (°C)	Substrate	ScN Orientation	ScN layer thickness (μm)	FWHM (arcsec)
Reactive magnetron sputter deposition[31]	750	MgO (001)	(002)	0.345	3132
Reactive magnetron sputter deposition[31]	750	MgO (001)	(111)	0.345	7668
MBE[32]	600–1000	Si (111)	(111)	0.225	1983–7900
rf-MBE[25]	800	Si (100)	(100)	0.8	2520
dc-Reactive magnetron sputtering[33]	850	MgO (001)	(001)	0.48–0.52	2430
RSMBE[9]	300–850	MgO (100)	(200)	0.12–0.320	1260–2340
GSMBE[22]	800	3C-SiC (111)/6H-SiC(0001)	(111)	0.2	1047
dc-Reactive magnetron sputtering[34]	650	MgO (001)	(001)	0.47–0.52	2487–2754
MBE[24]	750–900	MgO (110)	(220)	0.1–0.15	1800–2520
MBE[24]	750–900	α-Al2O3 (1010)	(110)	0.1–0.15	1760–3960
Present work by PVT	1850–2000	W (100)	(200)	14–90	821–1438

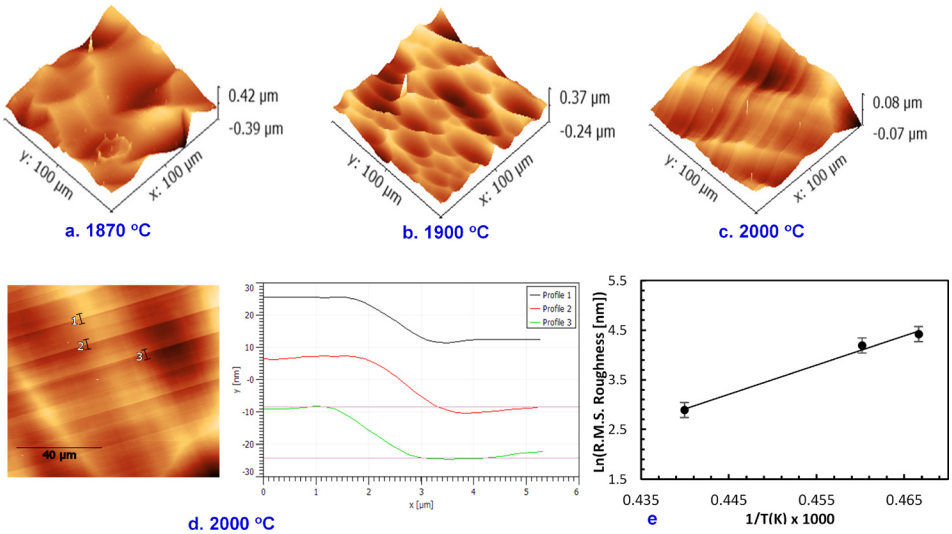

FIG. 5. AFM images of ScN grown at different temperatures and at 15 Torr. Plot (e) represents the effect of growth temperature on the surface roughness.

surface diffusion distance. In the case of formation of steps, the average distance between neighboring kinks is far smaller than the average surface diffusion distance of the adatoms.[30] In other words, the step velocity is higher than the diffusion speed of adatoms. When the kink density is adequately high, steps perform as holes through which adatoms can be drawn in a continuous flow.

The surface morphologies of the ScN layers grown at different temperatures, are compared in Fig. 5. The morphology of the ScN crystal surface was uniform at different growth temperatures, and well-ordered steps with a step height of about 15 nm were observed when temperature was increased to 2000 °C. The surface roughness of the ScN films decreased from 83 nm to 18 nm as the growth temperature was increased from 1870 °C to 2000 °C because the adatom mobility increases with temperature. The relationship between the log of the film roughness and inverse temperature was linear. This trend indicates that the inverse relationship is a consequence of the thermally activated process which is in accordance with the limited adatom mobility at lower temperature. AFM and SEM showed that the ScN surface consisted of both nanometer steps [Fig. 5(d)] and much larger micrometer scale steps (Fig. 4).

ScN (200) single crystals were grown on W (100) by the physical vapor transport method in the temperature range of 1850–2000 °C. Out-of-plane θ-2θ and in-plane ϕ x-ray diffraction scans revealed the epitaxial growth of ScN with a cube-on-cube plane relationship ScN (200) || W (200) and with normal direction ScN [200] || W [110]. The crystal surface exhibited layer-by-layer fashion with steps, and cracks formed due to the difference in the thermal expansion between ScN and W. AFM showed that the growth temperature had a dramatic impact on the roughness of the crystal with an inverse relationship. The x-ray rocking curve (XRC) showed that the crystal quality is excellent compared to the previously reported qualities, and FWHM of ScN produced in this work is the lowest value reported to date.

Support for this project from the National Science Foundation Division of Materials Research (Award No. 1508172) and Higher Committee for Education Development in Iraq is greatly appreciated. This material is based upon work supported by the National Science Foundation under CHE-1621665.

[1]P. Eklund, S. Kerdsongpanya, and B. Alling, J. Mater. Chem. C **4**, 3905 (2016).
[2]Z. Gu, J. H. Edgar, J. Pomeroy, M. Kuball, and D. W. Coffey, J. Mater. Sci.: Mater. Electron. **15**, 555 (2004).
[3]J. P. Dismukes, W. M. Yim, J. J. Tietjen, and R. E. Novak, RCA Rev. **31**, 680 (1970).
[4]J. P. Dismukes, W. M. Yim, and V. S. Ban, J. Cryst. Growth **13–14**, 365 (1972).
[5]W. Lengauer, J. Solid State Chem. **76**, 412 (1988).
[6]D. Gall, M. Stoehr, and J. E. Greene, Phys. Rev. B **64**, 174302 (2001).
[7]M. A. Moram, Z. H. Barber, C. J. Humphreys, T. B. Joyce, and P. R. Chalker, J. Appl. Phys. **100**, 023514 (2006).
[8]Y. Kumagai, N. Tsunoda, and F. Oba, Phys. Rev. Appl. **9**, 034019 (2018).
[9]T. Ohgaki, K. Watanabe, Y. Adachi, I. Sakaguchi, S. Hishita, N. Ohashi, and H. Haneda, J. Appl. Phys. **114**, 093704 (2013).
[10]B. Saha, M. Garbrecht, J. A. Perez-Taborda, M. H. Fawey, Y. R. Koh, A. Shakouri, M. Martin-Gonzalez, L. Hultman, and T. D. Sands, Appl. Phys. Lett. **110**, 252104 (2017).
[11]G. V. Samsonov, M. D. Lyutaya, and V. S. Neshpor, Zh. Prikl. Khim. **36**, 2108 (1963).
[12]N. Sclar, J. Appl. Phys. **35**, 1534 (1964).
[13]K. A. Gschneidner, in *Scandium: Its Occurrence, Chemistry, Physics, Metallurgy, Biology, and Technology*, edited by C. T. Horovitz (Academic Press, London, New York, 1975), p. 165.
[14]M. A. Moram, M. J. Kappers, T. B. Joyce, P. R. Chalker, Z. H. Barber, and C. J. Humphreys, J. Cryst. Growth **308**, 302 (2007).
[15]L. Lupina, M. H. Zoellner, T. Niermann, B. Dietrich, G. Capellini, S. B. Thapa, M. Haeberlen, M. Lehmann, P. Storck, and T. Schroeder, Appl. Phys. Lett. **107**, 201907 (2015).
[16]T. Lei, T. D. Moustakas, R. J. Graham, Y. He, and S. J. Berkowitz, J. Appl. Phys. **71**, 4933 (1992).
[17]T. L. Chu, J. M. Jackson, A. E. Hyslop, and S. C. Chu, J. Appl. Phys. **42**, 420 (1971).
[18]R. Kaplan, S. M. Prokes, S. C. Binari, and G. Kelner, Appl. Phys. Lett. **68**, 3248 (1996).
[19]M. Akiyama, T. Kamohara, K. Kano, A. Teshigahara, Y. Takeuchi, and N. Kawahara, Adv. Mater. **21**, 593 (2009).
[20]Y. Lu, M. Reusch, N. Kurz, A. Ding, T. Christoph, M. Prescher, L. Kirste, O. Ambacher, and A. Žukauskaitė, APL Mater. **6**, 076105 (2018).
[21]J. H. Edgar, T. Bohnen, and P. R. Hageman, J. Cryst. Growth **310**, 1075 (2008).
[22]S. W. King, R. F. Davis, and R. J. Nemanich, J. Vac. Sci. Technol. A **32**, 061504 (2014).
[23]D. Gall, M. Städele, K. Järrendahl, I. Petrov, P. Desjardins, R. T. Haasch, T.-Y. Lee, and J. E. Greene, Phys. Rev. B **63**, 125119 (2001).
[24]T. Ohgaki, I. Sakaguchi, N. Ohashi, and H. Haneda, J. Cryst. Growth **476**, 12 (2017).

[25]M. A. Moram, S. V. Novikov, A. J. Kent, C. Nörenberg, C. T. Foxon, and C. J. Humphreys, J. Cryst. Growth **310**, 2746 (2008).
[26]T. Kimoto, Prog. Cryst. Growth Charact. Mater. **62**, 329 (2016).
[27]J. H. Edgar, L. Liu, B. Liu, D. Zhuang, J. Chaudhuri, M. Kuball, and S. Rajasingam, J. Cryst. Growth **246**, 187 (2002).
[28]L. Du, J. H. Edgar, E. A. Kenik, and H. Meyer, J. Mater. Sci.: Mater. Electron. **21**, 78 (2010).
[29]H. A. Al Atabi, Z. F. Al Auda, B. Padavala, M. Craig, K. Hohn, and J. H. Edgar, Cryst. Growth Des. **18**, 3762 (2018).
[30]Y. Li, X. Chen, and J. Su, Appl. Surf. Sci. **371**, 242 (2016).
[31]D. Gall, I. Petrov, N. Hellgren, L. Hultman, J. E. Sundgren, and J. E. Greene, J. Appl. Phys. **84**, 6034 (1998).
[32]M. A. Moram, T. B. Joyce, P. R. Chalker, Z. H. Barber, and C. J. Humphreys, Appl. Surf. Sci. **252**, 8385 (2006).
[33]P. V. Burmistrova, J. Maassen, T. Favaloro, B. Saha, S. Salamat, Y. R. Koh, M. S. Lundstrom, A. Shakouri, and T. D. Sands, J. Appl. Phys. **113**, 153704 (2013).
[34]P. V. Burmistrova, D. N. Zakharov, T. Favaloro, A. Mohammed, E. A. Stach, A. Shakouri, and T. D. Sands, J. Mater. Res. **30**, 626 (2015).